





Posttranscriptional regulation of colonic epithelial repair by RNA binding protein IMP1/IGF2BP1

Priya Chatterji¹, Patrick A Williams², Kelly A Whelan^{3,4}, Fernando C Samper^{5,6} , Sarah F Andres¹, Lauren A Simon², Louis R Parham², Rei Mizuno¹, Emma T Lundsmith⁷, David SM Lee⁸, Shun Liang⁹, HR Sagara Wijeratne⁹, Stefanie Marti^{4,5}, Lillian Chau¹, Veronique Giroux¹⁰, Benjamin J Wilkins¹¹, Gary D Wu¹, Premal Shah^{9,12} , Gian G Tartaglia^{5,6,13}  & Kathryn E Hamilton^{2,*} 

Abstract

RNA binding proteins, including IMP1/IGF2BP1, are essential regulators of intestinal development and cancer. *Imp1* hypomorphic mice exhibit gastrointestinal growth defects, yet the specific role for IMP1 in colon epithelial repair is unclear. Our prior work revealed that intestinal epithelial cell-specific *Imp1* deletion (*Imp1^{ΔIEC}*) was associated with better regeneration in mice after irradiation. Here, we report increased IMP1 expression in patients with Crohn's disease and ulcerative colitis. We demonstrate that *Imp1^{ΔIEC}* mice exhibit enhanced recovery following dextran sodium sulfate (DSS)-mediated colonic injury. *Imp1^{ΔIEC}* mice exhibit Paneth cell granule changes, increased autophagy flux, and upregulation of *Atg5*. *In silico* and biochemical analyses revealed direct binding of IMP1 to *MAP1LC3B*, *ATG3*, and *ATG5* transcripts. Genetic deletion of essential autophagy gene *Atg7* in *Imp1^{ΔIEC}* mice revealed increased sensitivity of double-mutant mice to colonic injury compared to control or *Atg7* single mutant mice, suggesting a compensatory relationship between *Imp1* and the autophagy pathway. The present study defines a novel interplay between IMP1 and autophagy, where IMP1 may be transiently induced during damage to modulate colonic epithelial cell responses to damage.

Keywords colonic repair; IGF2BP1; IMP1; inflammatory bowel disease; RNA binding protein

Subject Categories Autophagy & Cell Death; Molecular Biology of Disease; Protein Biosynthesis & Quality Control

DOI 10.15252/embr.201847074 | Received 14 September 2018 | Revised 27 March 2019 | Accepted 2 April 2019 | Published online 6 May 2019

EMBO Reports (2019) 20: e47074

Introduction

Intestinal epithelium maintains its integrity through orchestration of self-renewal, proliferation, differentiation, and cell death. The rapidity with which intestinal epithelium must respond to environmental stressors suggests a necessity for multiple layers of gene regulation. RNA binding proteins have emerged as critical regulators of intestinal proliferation and stem cell dynamics [1–7]. *IGF2* mRNA-binding protein 1 (IMP1, IGF2BP1) is an RNA binding protein with roles in mRNA trafficking, localization, and stability. Target mRNAs of IMP1 (orthologues include CRD-BP, ZBP1) include *IGF2*, *ACTB*, *MYC*, *H19*, *CD44*, *GLI1*, and *PTGS2* [8–15]. *In vitro* studies demonstrate that IMP1 forms stable complexes with its target mRNAs, confining these transcripts to ribonucleoprotein particles (RNPs) and stabilizing mRNA or inhibiting translation [13,14,16–23]. IMP1 also plays a functional role in mRNA transport to aid in cellular processes including movement and polarity [13,24]. Photoactivatable ribonucleoside-enhanced crosslinking and immunoprecipitation (PAR-CLIP) and enhanced crosslinking and immunoprecipitation (eCLIP) studies have identified a myriad of IMP1 targets, providing important insight into the diverse roles of IMP1 via regulation of specific transcripts [25,26]. Finally, recent reports suggest that IMP proteins are “readers” of N 6-methyladenosine (m⁶A) modified mRNAs,

1 Division of Gastroenterology, Department of Medicine, University of Pennsylvania Perelman School of Medicine, Philadelphia, PA, USA

2 Division of Gastroenterology, Hepatology, and Nutrition, Department of Pediatrics, Children's Hospital of Philadelphia, University of Pennsylvania Perelman School of Medicine, Philadelphia, PA, USA

3 Department of Pathology & Laboratory Medicine, Lewis Katz School of Medicine at Temple University, Philadelphia, PA, USA

4 Fels Institute for Cancer Research & Molecular Biology, Lewis Katz School of Medicine at Temple University, Philadelphia, PA, USA

5 Centre for Genomic Regulation (CRG), The Barcelona Institute of Science and Technology, Barcelona, Spain

6 Universitat Pompeu Fabra (UPF), Barcelona, Spain

7 Thomas Jefferson Medical College, Thomas Jefferson University, Philadelphia, PA, USA

8 Genomics and Computational Biology Graduate Group, Perelman School of Medicine, University of Pennsylvania, Philadelphia, PA, USA

9 Department of Genetics, Rutgers University, New Brunswick, NJ, USA

10 Department of Anatomy and Cell Biology, Faculty of Medicine and Health Sciences, Universite de Sherbrooke, Sherbrooke, QC, Canada

11 Department of Pathology and Laboratory Medicine, Children's Hospital of Philadelphia, Philadelphia, PA, USA

12 Human Genetics Institute of New Jersey, Piscataway, NJ, USA

13 Institutio Catalana de Recerca i Estudis Avancats (ICREA), Barcelona, Spain

*Corresponding author. Tel: +267-426-5266; Fax: +267-426-7814; E-mail: hamiltonk1@email.chop.edu

which may impart binding and functional specificity of IMPs to regulate mRNA storage and stability [27].

In mice, *Imp1* is expressed in the small intestine and colon during embryonic development through postnatal day 12 and at low levels during adulthood [28]. *Imp1* hypomorphic mice exhibit dwarfism, intestinal defects, and perinatal lethality [28,29]. In these mice, development of the intestine was impaired and mucosal thickness was significantly reduced. These mice had diminished villi and crypts which was associated with severe malabsorption, but no obvious impairment of cellular lineages. Recent studies in the fetal mouse brain implicate *Imp1* as a regulator of differentiation of stem/progenitor cells, where *Imp1* deletion leads to neural stem cell depletion [30]. In adult mouse colon, IMP1 is expressed in the epithelial crypt base and in mesenchymal cells following injury [15,31]. Our prior published studies demonstrated that IMP1 may promote or suppress colon tumorigenesis based upon its expression and function in the epithelial or mesenchymal compartments, underscoring the notion that IMP1 may exhibit opposing effects in different contexts [32,33]. Taken together, prior *in vivo* studies suggest that IMP1 is a key regulator of development and cancer, potentially via regulation of stem/progenitor cell maintenance [34]. We recently demonstrated that *Imp1* is expressed in intestinal epithelial stem cells and that *Imp1* deletion in these cells promotes enhanced regeneration following whole body irradiation, suggesting that *Imp1* may play an integral role in modulating tissue damage responses in the gut [35].

Prior *in vitro* reports have suggested a role for IMP1 in cellular stress response. Studies of the IMP1 chicken orthologue, ZBP1, revealed an essential role in the integrated stress response (ISR) via differential regulation of mRNA fates in non-stressed versus stressed cells [18]. Characterization of IMP1 RNP granules *in vitro* revealed enrichment of mRNAs encoding proteins involved in the secretory pathway, ER stress, and ubiquitin-dependent metabolism [36]. Furthermore, evaluation of processing bodies (P-bodies) using fluorescence-activated particle sorting (FAPS) demonstrated enrichment of IMP1 together with translationally repressed mRNAs, suggesting that IMP1 may stabilize and/or repress target mRNAs [37]. Despite its considerable importance in normal development and its role in coordinating cellular stress, the specific mechanistic roles of IMP1 in adult tissues have yet to be elucidated *in vivo*. The focus and goal for the present study is to demonstrate functional roles of IMP1 in the adult gastrointestinal epithelium (where IMP1 is dynamically expressed following damage) in order to understand how these findings may be relevant to human disease.

Results

IMP1 is upregulated in patients with Crohn's disease and ulcerative colitis

Previous studies demonstrated that *Imp1* exhibits heterochronic expression in mice during development, has low expression in adult tissues, and is highly expressed in multiple cancers. Our recent study revealed *Imp1* upregulation in intestinal epithelial cells in response to whole body irradiation [35]; however, the

mechanistic role for *Imp1* in regulating epithelial damage remains unknown. We evaluated whole tissue biopsies from adult patients with Crohn's disease and ulcerative colitis (Table 1) in order to ascertain IMP1 expression in human disease. We observed a > 5-fold increase in *IMP1* RNA levels in both Crohn's disease (5.3 ± 1.81) and ulcerative colitis mucosal biopsies as compared to those from control subjects (6.6 ± 2.6 ; Fig 1A). We confirmed IMP1 overexpression in patients with Crohn's disease via immunohistochemistry, where we observed both epithelial and stromal IMP1 staining and confirmed little or absent IMP1 expression in healthy control patients (Fig 1B). Consistent with these findings, analysis of published the Pediatric RISK Stratification Study (RISK) cohort of RNA-sequencing data [38] from pediatric patients with Crohn's disease (CD) patients revealed that *IMP1* is upregulated significantly compared to control patients and that this effect is specific to *IMP1* (i.e., other distinct isoforms, *IMP2* and *IMP3*, are not changed; Fig 1C).

Table 1. Patient demographics.

Analysis	Type	Sex	Age
qPCR	Control	Female	66
	Control	Male	64
	Control	Male	76
	Control	Male	61
	Control	Male	62
	Control	No info given	No info given
	CD	Male	21
	CD	Female	73
	CD	Female	28
	CD	Male	20
	CD	Female	32
	CD	Female	22
	CD	No info given	No info given
	CD	Female	49
	UC	Male	74
	UC	Male	32
	UC	Male	30
	IHC	UC	Female
UC		Male	64
UC		Female	56
Control		Female	40
Control		Male	38
Control		Male	47
Control		Male	54
CD		Male	65
CD		Female	66
CD		Female	61
CD	Female	55	

CD, Crohn's disease; IHC, Immunohistochemistry; UC, Ulcerative colitis.

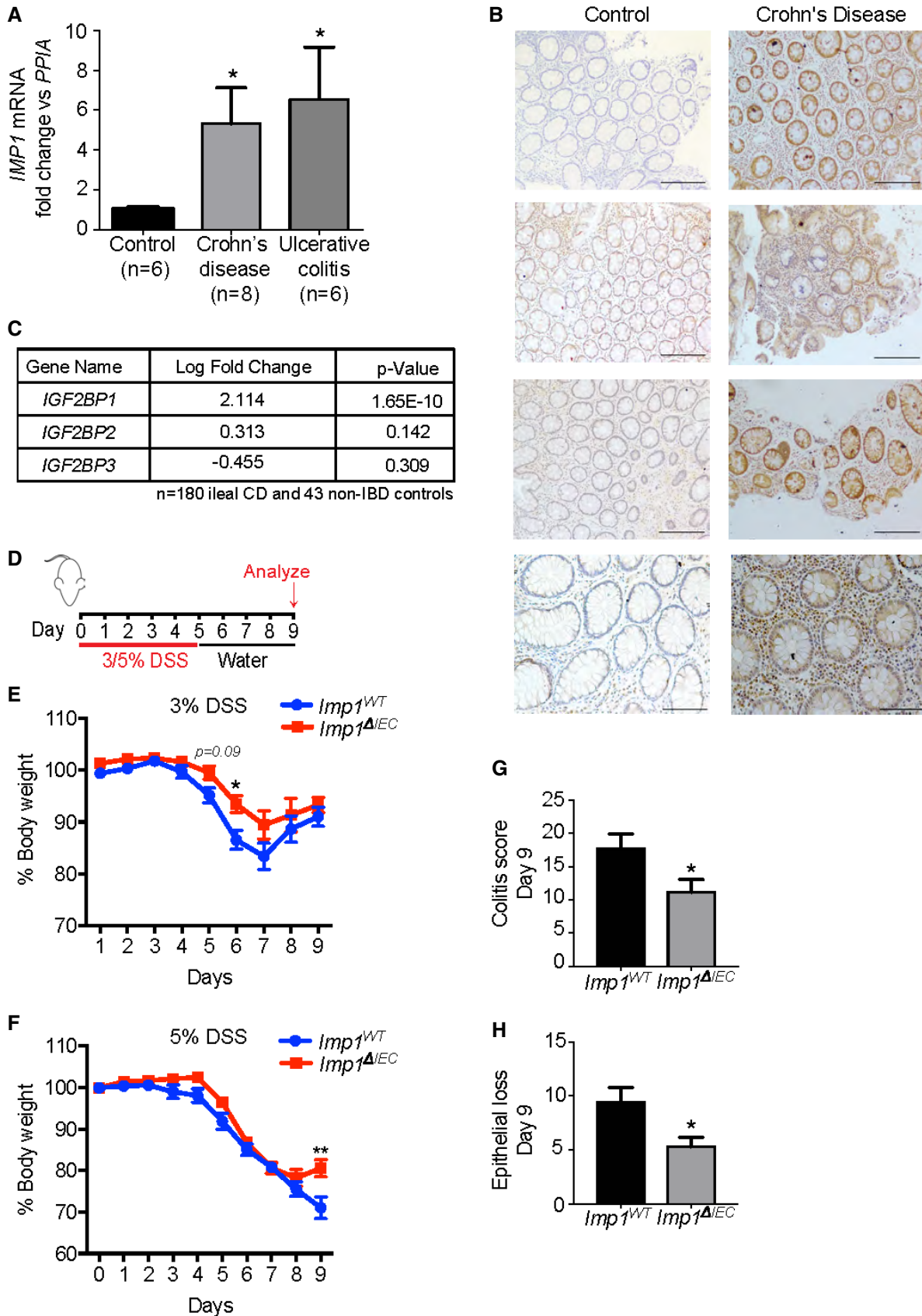


Figure 1.

Figure 1. IMP1 is upregulated in patients with Crohn's disease and ulcerative colitis.

- A qPCR analysis for *IMP1* expression in colon biopsy samples from adult ulcerative colitis (UC) and Crohn's disease (CD) patients. *IMP1* expression is > 5-fold higher in UC (6.554 ± 2.609 , $n = 6$; P -value = 0.0302) and CD samples (5.314 ± 1.807 , $n = 8$; P -value = 0.0343) as compared to control samples (1 ± 0.1245 , $n = 6$).
- B Representative immunohistochemistry demonstrating *IMP1* expression in colon biopsy samples from CD patients and normal adults (Scale bars = 500 μ m).
- C Differential gene expression analysis of pediatric ileal CD patient samples ($n = 180$) shows increased (> 4-fold) *IMP1* expression as compared to non-inflammatory bowel disease (IBD) pediatric samples ($n = 43$).
- D Experiment schematic. Mice were given either 3% or 5% dextran sodium sulfate (DSS) in drinking water for 5 days followed by 4 days of recovery.
- E With 3% DSS, mice with *Imp1* deletion [*Imp1*^{AIEC} ($n = 8$)] lost significantly less weight compared to controls (*Imp1*^{WT} ($n = 18$); P -value = 0.0259 at day 6).
- F With 5% DSS, *Imp1*^{AIEC} mice began to regain weight at day 9 compared to controls (*Imp1*^{WT} ($n = 22$) and *Imp1*^{AIEC} ($n = 16$; P -value = 0.0104).
- G *Imp1*^{AIEC} mice show significantly less total colitis (11.14 ± 1.933 , $n = 7$; scored blinded by a pathologist) as compared to *Imp1*^{WT} mice (17.75 ± 2.144 , $n = 8$) after 5% DSS (P -value = 0.0415).
- H *Imp1*^{AIEC} mice show significantly less epithelial loss (5.286 ± 0.865 , $n = 7$) as compared to *Imp1*^{WT} mice (9.375 ± 1.375 , $n = 8$) after 5% DSS (P -value = 0.0303).
- Data information: All data are expressed as mean \pm SEM. * $P < 0.05$; ** $P < 0.01$ by unpaired two-tailed t -test (for DSS weights, significance was determined using the Mann–Whitney test).

Intestinal epithelial *Imp1* deletion attenuates the effects of DSS-mediated colonic damage

Our recent publication revealed that mice with *Imp1* deletion in intestinal and colonic epithelium (*VillinCre; Imp1*^{f/f}, referred to as *Imp1*^{AIEC} mice; Fig EV1A) exhibit enhanced recovery following 12 Gy whole body irradiation, where *Imp1*^{AIEC} mice formed significantly more regenerative microcolonies in small intestine compared to control mice [35]. To determine the role for *Imp1* during colonic injury, we evaluated *Imp1*^{AIEC} mice using the dextran sodium sulfate (DSS) model, which leads to robust colonic epithelial damage (Fig 1D). *Imp1*^{WT} and *Imp1*^{AIEC} mice exhibited similar weight loss during initial days of 3% DSS treatment, but *Imp1*^{AIEC} mice exhibited less weight loss during recovery starting at day 6 (1 day following the cessation of DSS treatment, Fig 1E). We next evaluated mice treated with higher (5%) DSS levels and evaluated mice at day 5 when damage level is peak. While we did not observe significant differences in weight loss or histological colitis score between genotypes at day 5 of 5% DSS (Fig EV1B and C), we did observe that 5% DSS-treated *Imp1*^{AIEC} mice regain more weight at day 9 (4 days following the cessation of DSS, Fig 1F) and exhibited significantly lower histological colitis and epithelial loss scores compared to controls at this key time point in epithelial recovery (Fig 1G and H). Taken together, these data suggest that *IMP1* is robustly upregulated during chronic inflammation in patients with inflammatory bowel disease and mice with intestinal epithelial *Imp1* deletion exhibit an increase in recovery following acute colonic damage.

We next evaluated *Imp1*^{AIEC} mice during chronic DSS (Fig 2A). We found that *Imp1*^{AIEC} mice exhibited less weight loss at the termination of the chronic DSS protocol compared to controls (Fig EV1B–D), and this was associated with a significant decrease in histological colitis, inflammation, hyperplasia, and mononuclear cell score in *Imp1*^{AIEC} mice (Fig 2B–E). In addition, expression of *Il6*, *Il11*, *Tnf*, *Il1b*, and *Ifng* cytokines in colonic tissue was decreased in *Imp1*^{AIEC} mice (Fig 2F–J). Together, these observations suggest that *Imp1* loss in colonic epithelium is associated with an attenuated response to chronic, DSS-induced epithelial damage, allowing for better regeneration following inflammation. Because *Imp1* loss was associated with less damage/better repair, we evaluated whether *Imp1*^{AIEC} mice were more susceptible to inflammation (DSS)-associated tumorigenesis [39]. We subjected mice to the azoxymethane (AOM)-DSS model of colitis-associated tumorigenesis to determine the phenotypic consequence of *Imp1* deletion upon

tumor growth (Fig 2K). We did not observe a significant difference in tumor number, size, or load between the *Imp1*^{WT} and *Imp1*^{AIEC} mice (Fig 2L–N). This is intriguing, since our prior studies demonstrated that stromal *Imp1* deletion was associated with enhanced tumor growth [33]. Taken together, the present findings suggest that colonic epithelial cells with *Imp1* deletion regenerate better following damage than mice with wild-type *Imp1*; however, these mechanisms do not render *Imp1*^{AIEC} mice more or less susceptible AOM-DSS tumorigenesis.

IMP1 deletion is associated with changes in mRNA abundance and translation efficiency

Our finding that *Imp1*^{AIEC} mice exhibit better regeneration after chronic DSS compelled us to evaluate putative pathways underlying this phenotype. We demonstrated recently that *IMP1* deletion in LIN28B overexpression cells is associated with global changes in translation efficiency [35]. We therefore used ribosome profiling to evaluate changes in protein translation in the SW480 colorectal cancer cells with *IMP1* deletion (Fig EV1E). Following deep sequencing to compare total RNA abundance, RNA fragments protected by bound ribosomes (ribosome protected fragments, RPFs) were sequenced to define actively translating mRNAs (Data deposited in GEO (GSE112305) [NCBI tracking system #18999297]). We found that *IMP1* deletion affected gene expression at both mRNA abundance and RPF levels. Of the 10,043 genes analyzed, 7,386 exhibited no change in mRNA abundance or RPFs. We observed that 642 transcripts were exclusively changed at the mRNA abundance level, whereas 1,264 genes were changed only at the RPF level. The rest of the genes were regulated on both the mRNA abundance and RPF level (Fig 3A).

Translational efficiency of a gene is defined as the ratio of abundance in RPF to that of total mRNA abundance for a gene [40]. Cells with *IMP1* deletion exhibited differential translational efficiency for 1,469 genes (all translational efficiency data is listed in Dataset EV1). Pathway enrichment analysis for genes with differential translational efficiency [41] revealed a significant representation of pathways linked to cell cycle, gene expression and RNA processing, post-translational modification, autophagy, and metabolism (Fig 3B and Table EV1). These analyses (i) support the concept that *IMP1* levels can globally affect mRNA abundance and translation efficiency, and (ii) compelled us to consider autophagy as a putative pathway underlying a role for *IMP1* in colonic epithelial repair

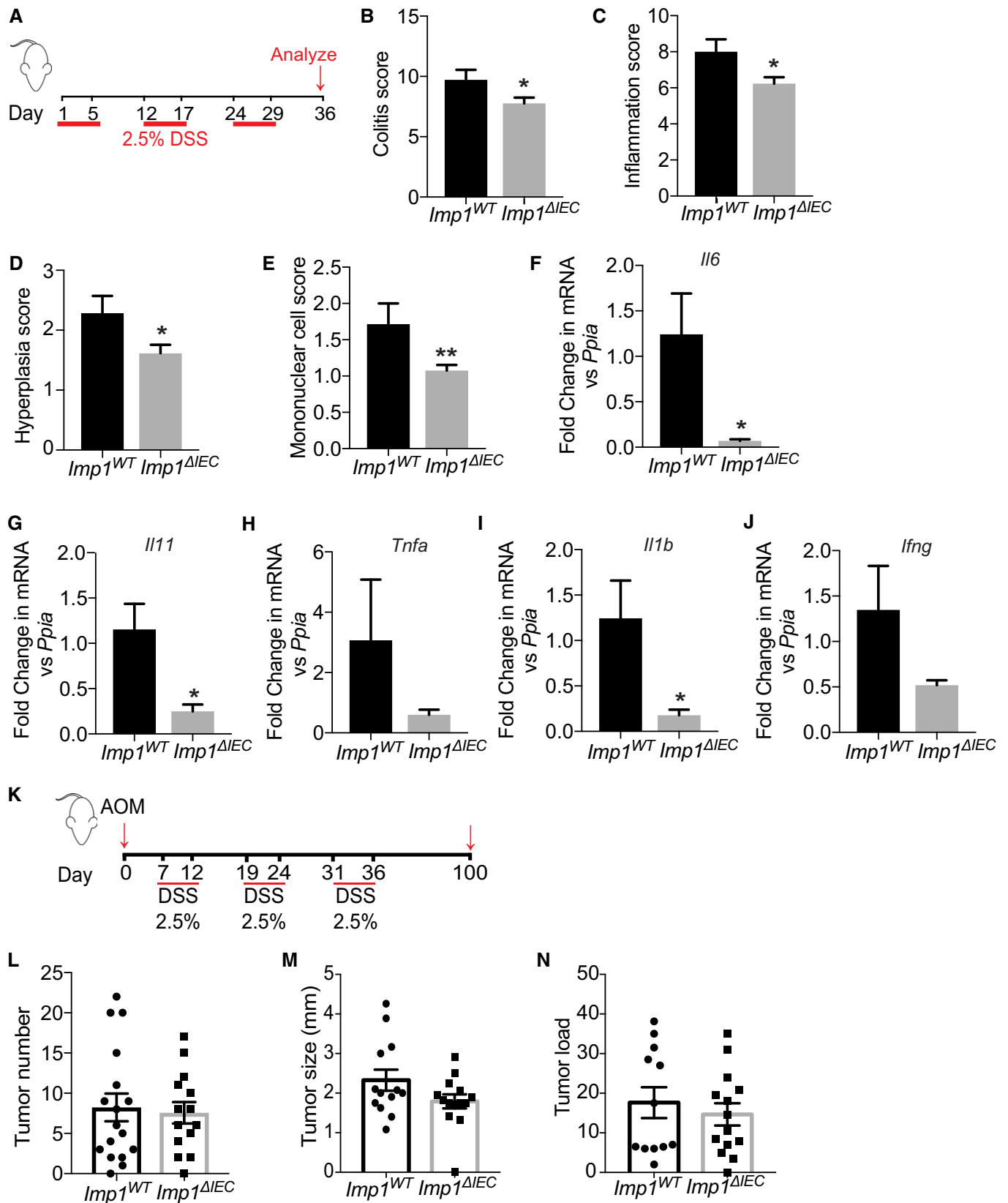
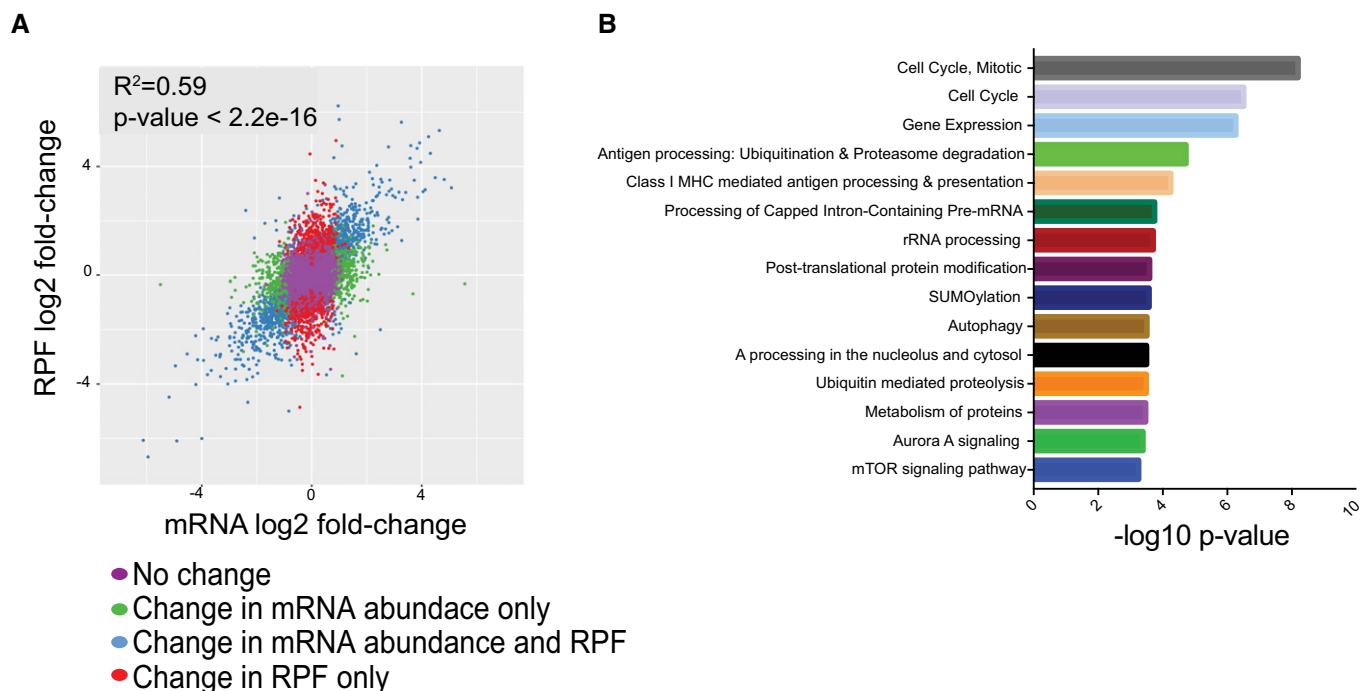


Figure 2.

Figure 2. Intestinal epithelial *Imp1* deletion attenuates the effects of DSS-mediated colonic damage.

- A Mice were given three cycles of 2.5% dextran sodium sulfate (DSS) in drinking water for 5 days followed by a week of recovery. Mice were analyzed at day 36.
- B *Imp1^{ΔIEC}* mice show significantly less total colitis (7.769 ± 0.4824 , $n = 13$; scored blinded by a pathologist) as compared to *Imp1^{WT}* mice (9.714 ± 0.8371 , $n = 7$; P -value = 0.0435).
- C *Imp1^{ΔIEC}* mice show significantly less hyperplasia (1.615 ± 0.1404 , $n = 13$) as compared to *Imp1^{WT}* mice (2.286 ± 0.2857 , $n = 7$; P -value = 0.0287).
- D *Imp1^{ΔIEC}* mice show significantly less inflammation score (6.231 ± 0.3608 , $n = 13$) as compared to *Imp1^{WT}* mice (8 ± 0.6901 , $n = 7$; P -value = 0.0213).
- E *Imp1^{ΔIEC}* mice show significantly less mononuclear cell infiltration (1.077 ± 0.076 , $n = 13$) as compared to *Imp1^{WT}* mice (1.714 ± 0.2857 , $n = 7$; P -value = 0.0128).
- F–J qPCR data showing cytokine expression following chronic DSS treatment in colon epithelium of *Imp1^{WT}* ($n = 4$) and *Imp1^{ΔIEC}* mice ($n = 6$) at day 36 (P -values are as follows: 0.0109 for *Il6*, 0.0107 for *Il11*, and 0.0240 for *Il1b*).
- K Tumors were induced in *Imp1^{WT}* and *Imp1^{ΔIEC}* mice using the azoxymethane/dextran sodium sulfate (AOM/DSS) model.
- L Tumors were evaluated 14 weeks after the initial AOM injection. *Imp1^{WT}* (8.235 ± 1.723 , $n = 17$, 5F/12M) and *Imp1^{ΔIEC}* (7.571 ± 1.337 , $n = 14$, 7F/7M) mice do not show any significant difference in tumor initiation.
- M, N *Imp1^{WT}* and *Imp1^{ΔIEC}* mice do not show any significant differences in tumor size or load. *Imp1^{WT}* $n = 17$, 5F/12M; *Imp1^{ΔIEC}* $n = 12$, 7F/7M.
- Data information: Data are expressed as mean \pm SEM. * $P < 0.05$, ** $P < 0.01$; by unpaired two-tailed t -test.

**Figure 3. IMP1 deletion increased level of proteins in the autophagy pathway.**

- A Scatterplot of differential expression between SW480 cells with and without *IMP1* deletion. The log₂ fold change between ribosome-bound RNAs (ribosome protected fragments, or RPF) and total mRNA is plotted. The plot indicates that *IMP1* loss is associated with changes in mRNA abundance and RPF.
- B Pathway analysis of genes with differential translational efficiencies between SW480 cells with and without *IMP1* deletion to define signaling/effector pathways that are enriched with *IMP1* deletion.

based upon evidence for autophagy as a protective mechanism in the gut [42–47].

Mice with *Imp1* deletion exhibit Paneth cell abnormalities and changes in epithelial cell autophagy

Despite significant morphological defects reported by others in *Imp1* hypomorphic mice, including villus blunting and misshapen crypts [28], we did not observe gross phenotypic changes in *Imp1^{ΔIEC}* mice where *Imp1* is lost solely in intestinal epithelial cells, which suggests that *IMP1* is dispensable in this epithelial compartment during homeostasis (Fig EV2A). We analyzed differentiated epithelial cell

types and did not observe differences in Paneth, goblet, or enteroendocrine cell numbers between genotypes (Fig EV2B–E); however, we observed diffuse lysozyme staining in *Imp1^{ΔIEC}* Paneth cells (Fig 4A and B), which we confirmed using transmission electron microscopy (Fig 4C).

Autophagy gene mutations have been associated with Paneth cell granule defects in patients with disease in numerous published studies [48–52]. We therefore evaluated autophagy levels in *Imp1^{ΔIEC}* mice. We performed western blotting for cleaved LC3 in freshly isolated colon and jejunum crypt cells, which contain stem, Paneth, and transit-amplifying cells. An increase in the lipidated form of cleaved LC3 (lower band) coupled with decreased expression of the

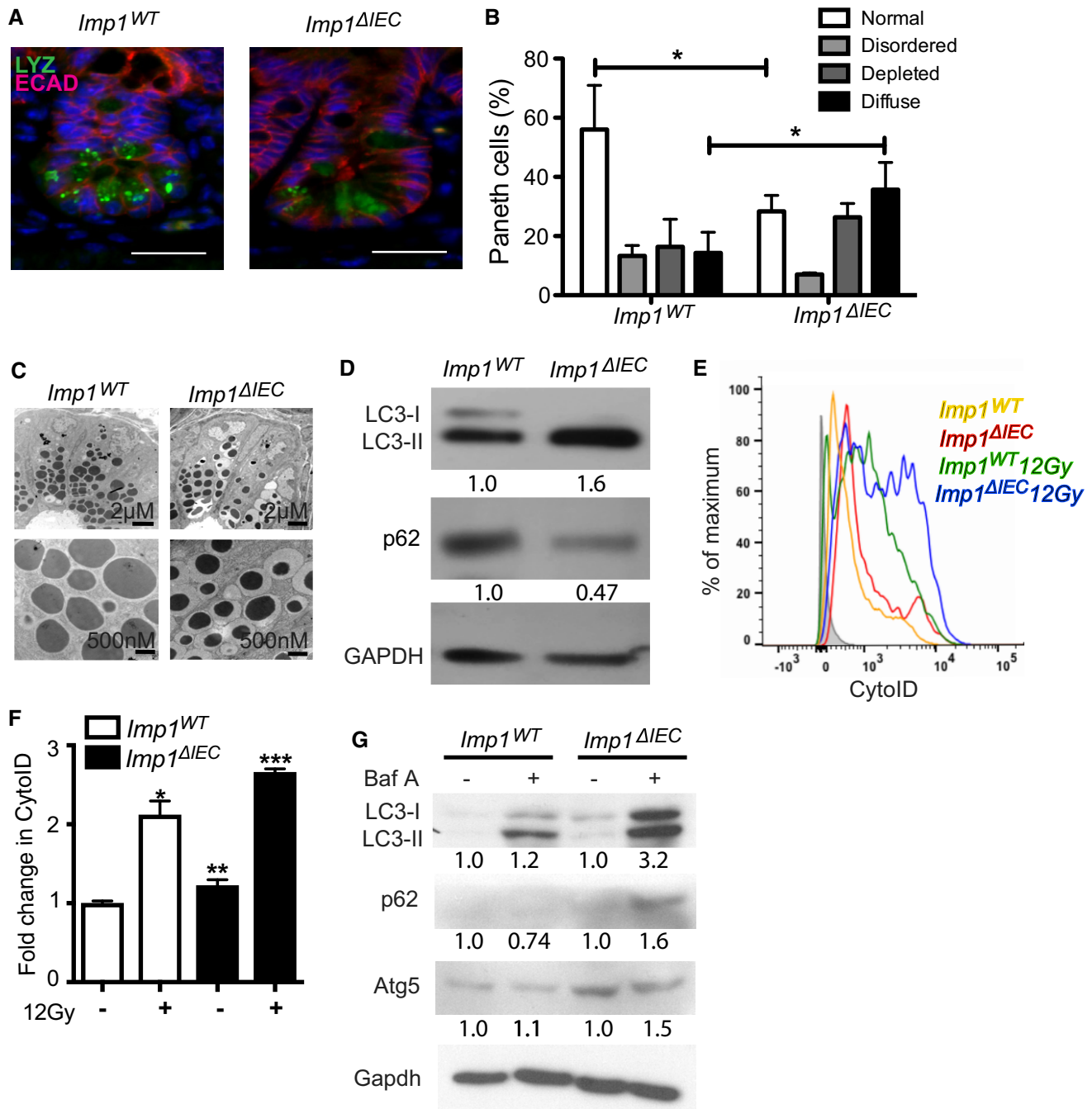


Figure 4. Mice with *Imp1* deletion exhibit Paneth cell abnormalities and changes in epithelial cell autophagy.

A Paneth cells from *Imp1*^{WT} and *Imp1*^{ΔIEC} mice were evaluated histologically using immunofluorescence (IF) for lysozyme (LYZ). E-cadherin (ECAD) staining was used to demarcate individual epithelial cells. Note presence of diffuse lysozyme staining in *Imp1*^{ΔIEC} mice. Scale bar = 25 μm.

B Published lysozyme scoring was utilized to evaluate specific Paneth cell phenotypes. *Imp1*^{ΔIEC} mice exhibit a significant shift from normal to diffuse lysozyme phenotype ($n = 4$ mice per genotype, blinded scoring; P -value = 0.0116).

C Transmission electron microscopy revealed an abundance of smaller, electron dense granules in *Imp1*^{ΔIEC} mice compared to control.

D Western blot for cleaved LC3 and p62 in colon epithelial cells from *Imp1*^{WT} and *Imp1*^{ΔIEC} mice. Blots are representative of three independent experiments with densitometry measurements listed below each band.

E, F Live cell staining of autophagic structures with the cationic amphiphilic tracer dye CytoID indicated a significant increase in autophagic vesicle content in crypt epithelial cells from *Imp1*^{ΔIEC} mice ($n = 8$) compared to *Imp1*^{WT} mice ($n = 7$) via flow cytometry (representative histogram plot in E).

G Crypt enteroids from control and *Imp1*^{ΔIEC} mice treated with Bafilomycin A1 for 12 h. Enteroids were washed with cold PBS and harvested in protein lysis buffer prior to immunoblot. Blot is representative of two independent experiments, representing independent enteroid lines. Densitometry measurements are listed below each band.

Data information: All data are expressed as mean ± SEM. * $P < 0.05$; ** $P < 0.01$, *** $P < 0.001$; by ordinary one-way ANOVA with Bonferroni's multiple comparison test (F) or unpaired two-tailed t-test (B).

autophagy cargo-associated protein p62 suggested that autophagy flux may be increased in *Imp1^{AIEC}* mice (Fig 4D colon; Fig EV2F jejunum) [53]. We observed concurrently a decrease in autophagy cargo-associated protein p62 in *Imp1^{AIEC}* colon crypts (Fig 4D). To evaluate changes in autophagy flux by a second method, we utilized freshly isolated, live crypt cells stained with the cationic amphiphilic tracer dye CytoID, which selectively labels autophagic structures [54–56]. We validated CytoID as a tool to measure autophagy in crypt cells via western blot and flow cytometry using *Atg7^{AIEC}* mice (Fig EV3A and B). CytoID analysis revealed an increase in basal autophagic vesicle content in *Imp1^{AIEC}* mice compared to *Imp1^{WT}*, an effect that was

amplified in live cells at day 4 recovery following 12 Gy irradiation (Fig 4E and F). We did not observe significant differences in cell viability between genotypes in this assay (Fig EV3C). Taken together, these data suggest that *Imp1^{AIEC}* mice exhibit modest, yet significant increases in basal autophagy flux in intestinal epithelium.

Ribosome profiling analysis demonstrating increased translation efficiency of the autophagy pathway with *IMP1* deletion was consistent with observed increases in LC3 protein levels in both *Imp1^{AIEC}* mice and *IMP1*-KO cells (Figs 4D and EV4A). We observed minimal differences in mRNA levels for autophagy genes *in vitro* or *in vivo* (Fig EV4B and C), except for *Atg3* and *ATG5*, which were increased

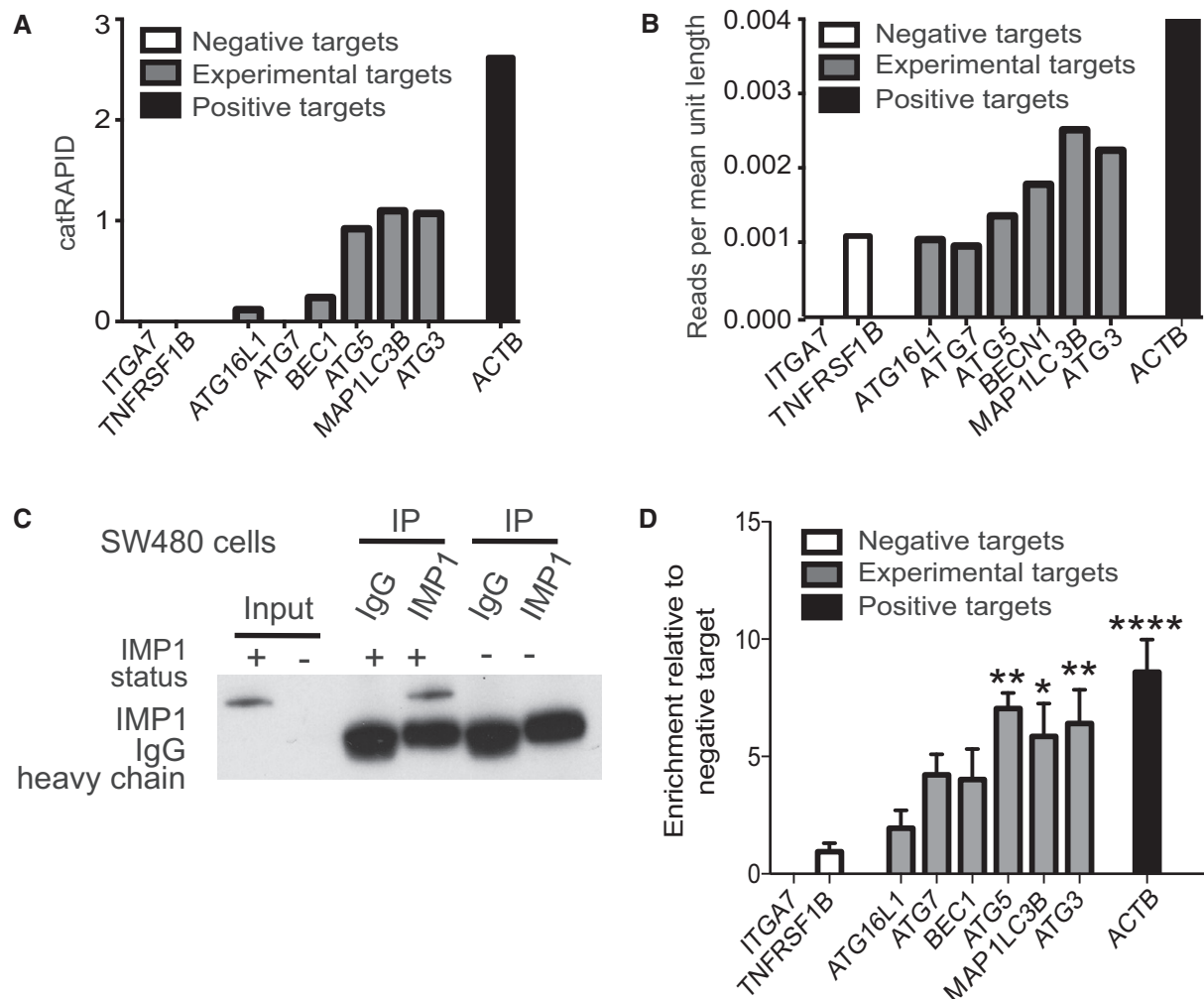


Figure 5. IMP1 interacts with autophagy transcripts.

A catRAPID transcript score. For each predicted transcript, we measured the IMP1 interaction propensity with respect to the negative control IgG. Negative targets (ITGA7 and TNFRSF1B) were also evaluated.

B We retrieved CLIP scores from published eCLIP data and compared against the same set of autophagy-related transcripts analyzed in (A) and found a strong correlation between catRAPID scores and eCLIP data ($r = 0.9838465$ Pearson correlation coefficient). CLIP data scores were calculated as total number of reads corresponding to the transcript divided by the length of the different isoforms.

C We evaluated binding of endogenous IMP1 to autophagy transcripts using RIP assays in SW480 cells ($n = 3$). Specific enrichment of IMP1 was confirmed by IP with either IMP1 or control IgG antibodies followed by western blot for IMP1. We used cells with IMP1 deletion as negative control.

D Enrichment of target transcripts over control is represented relative to negative target, TNFRSF1B. ACTB is the positive control (P -value < 0.0001 ; $n = 3$ independent experiments). The targets that are significant are ATG5 (P -value = 0.0013), MAP1LC3B (P -value = 0.0148), and ATG3 (P -value = 0.0052).

Data information: All data are expressed as mean \pm SEM. * $P < 0.05$; ** $P < 0.01$, **** $P < 0.0001$; by ordinary one-way ANOVA test or unpaired two-tailed t -test.

in vitro and *in vivo*, respectively. We found a significant increase in Atg5 protein levels in *Imp1^{ΔIEC}* mice as well (Fig EV4D). To evaluate autophagy flux, we assessed crypt enteroids from *Imp1^{ΔIEC}* mice in the presence of the Bafilomycin A, a lysosomotropic agent that inhibits autophagy. We observed a robust increase in cleaved LC3 and accumulated p62 in Bafilomycin A-treated *Imp1^{ΔIEC}* enteroids as compared to *Imp1^{WT}*, suggesting higher autophagy flux in knockout enteroids (Fig 4G). These data support *Imp1* in intestinal epithelium as a negative regulator of autophagy. Thus, dynamic regulation of *Imp1* may serve to modulate autophagy during the reparative response.

IMP1 interacts with autophagy transcripts

IMP1 is a pleiotropic protein that has been demonstrated to bind directly to a large number of transcripts in cell lines [26,57]. We therefore evaluated putative interactions between IMP1 protein and autophagy transcripts. We first performed *in silico* analyses to assess binding propensities of IMP1 for autophagy transcripts using catRAPID (fast predictions of RNA and protein interactions and domains at the Center for Genomic Regulation, Barcelona, Catalonia), which predicts RNA:protein interactions based upon nucleotide and polypeptide sequences as well as physicochemical properties [58]. These analyses predicted binding of IMP1 to *BECN1*, *MAP1LC3B*, and *ATG3* transcripts (Fig 5A), as well as the positive control *ACTB*. IMP1 binding was also predicted to *ATG16L1*, *ATG7*, and *ATG5*, albeit with low binding scores. This algorithm predicted no binding to negative targets *TNFRSF1B* and *ITGA7* [26]. We next evaluated published IMP1 eCLIP data [26] for the same autophagy transcripts and found positive binding (Fig 5B). We interrogated published eCLIP data for binding location of autophagy transcripts and found that all IMP1 reads on autophagy transcripts were localized on untranslated regions (UTR) regions. Specifically, these analyses revealed IMP1 binding on the 5'UTR for *ATG3*, *ATG5*, and *BECN1* and 3'UTR for *ATG16L1*, *ATG7*, and *MAP1LC3B* (Table 2).

To evaluate IMP1 binding to these targets in colon cancer cell lines, we performed ribonucleoprotein (RNP)-immunoprecipitation with antibodies to endogenous IMP1 in SW480 (Fig 5C) and Caco2 cells (Fig EV4E and F). Previously confirmed IMP1 target *ACTB* and negative targets *TNFRSF1B* and *ITGA7* were used as positive and negative controls, respectively. We observed significant enrichment of IMP1 (normalized to input and then negative controls) binding to autophagy genes *MAP1LC3B*, *ATG5*, and *ATG3* (Fig 5D). *ATG7* and *BECN1* demonstrated higher enriched binding than negative controls, but these were not significant. Taken together, we demonstrate via three independent methods that IMP1 binds directly to a subset of autophagy transcripts, all of which are required early in the autophagy cascade.

Atg7 deletion augments the response of *Imp1^{ΔIEC}* mice to DSS-induced colonic damage

We reported recently that *Imp1^{ΔIEC}* mice recover more efficiently following 12 Gy whole body irradiation [35]. To evaluate the relative contribution of autophagy to colonic epithelial responses to DSS in *Imp1^{ΔIEC}* mice, we crossed *Imp1^{ΔIEC}* mice with mice harboring *Atg7*-floxed alleles (*Imp1^{ΔIEC}Atg7^{ΔIEC}*). *ATG7* is an essential component of the ATG conjugation system and is critical for early

Table 2. eCLIP binding analysis.

Transcript	Number of reads that bind to		
	5'UTR	CDS	3'UTR
MAP1LC3B	0	0	32
ATG3	25	0	0
ATG16L1	0	0	25
ATG7	0	0	86
ATG5	8	0	0
BECN1	20	0	0

CDS, coding determining region; UTR, untranslated regions.

autophagosome formation [59]. In addition, prior studies of intestinal epithelial-specific *Atg7* deletion demonstrated loss of autophagic vacuoles via transmission electron microscopy analysis similar to that of intestinal epithelial-specific knockout of the autophagy genes *Atg16L1* or *Atg5* [43,60]. Interestingly, we found upregulation of *Imp1* protein levels with *Atg7* deletion (Fig 6A). Prior studies suggest modest enhanced susceptibility to colitis in mice with genetic deletion of *Atg7* [61]. When *Atg7^{ΔIEC}* and *Imp1^{ΔIEC}Atg7^{ΔIEC}* mice were treated with 3% DSS and compared to experiments performed in Fig 1E, we found that *Imp1^{WT}*, *Imp1^{ΔIEC}*, and *Atg7^{ΔIEC}* mice exhibited modest weight differences during recovery, whereas *Imp1^{ΔIEC}Atg7^{ΔIEC}* mice exhibited rapid weight loss and did not recover (Fig 6B and C), suggesting a compensatory mechanism between *Imp1* and *Atg7*. Using a higher dose of 5% DSS, we observed that both *Atg7^{ΔIEC}* mice and *Imp1^{ΔIEC}Atg7^{ΔIEC}* mice became moribund more rapidly than *Imp1^{WT}* and *Imp1^{ΔIEC}* mice (Fig EV5A and B).

To determine whether concurrent deletion of *Imp1* and *Atg7* is associated with spontaneous inflammation, we aged these mice for 12 months and evaluated them for histological changes. Blinded examination of colon and small bowel sections revealed no difference between aged *Imp1^{WT}* and *Imp1^{ΔIEC}Atg7^{ΔIEC}* mice. *Imp1^{ΔIEC}CAtg7^{ΔIEC}* mice exhibited minimal foci of acute inflammation (neutrophils in < 5% of examined mucosa) in 3 of 8 colons and 7 of 8 small bowels; similar findings are seen in control colon (1 of 6) and small bowel (3 of 6; Fig 6D). There were no features that suggest spontaneous chronic enteritis in either group.

Discussion

In the current study, we evaluated roles for the RNA binding protein IMP1 to regulate tissue homeostasis in colonic epithelium. Prior *in vivo* studies have implicated IMP1's critical function in development, and we and others have demonstrated diverse roles for IMP1 in cancer [28,32,33,35]. The present study is the first to uncover *in vivo* mechanisms for IMP1 during colonic epithelial repair, which could have important implications in human disease. Indeed, we report that IMP1 is upregulated in patients with Crohn's disease and ulcerative colitis and that mice with *Imp1* loss exhibit enhanced repair following DSS-mediated damage.

RNA binding proteins can exhibit pleiotropic roles during homeostasis and stress. IMP1-containing RNP granules are localized around the nucleus and in cellular projections, containing mRNAs

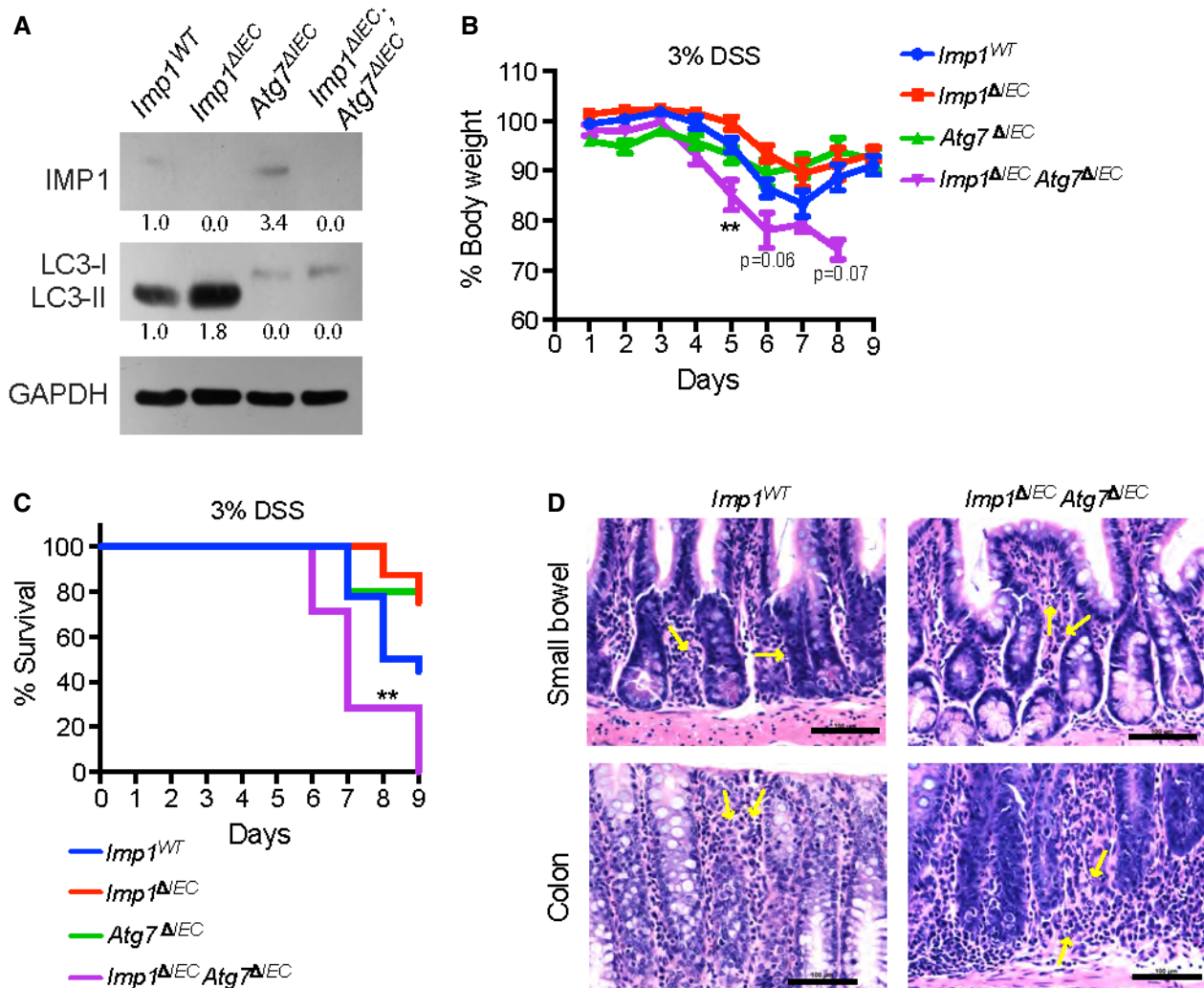


Figure 6. *Atg7* deletion augments the response of *Imp1*^{ΔIEC} mice to DSS-induced colonic damage.

A Representative western blot for cleaved LC3-II protein in mice with *Atg7* deletion (*Atg7*^{ΔIEC} and *Imp1*^{ΔIEC}; *Atg7*^{ΔIEC} mice). *Atg7*^{ΔIEC} mice also exhibit increase in IMP1 expression with densitometry measurements listed below each band.

B Evaluation of weight loss during 3% DSS and recovery for *Imp1*^{WT} ($n = 18$), *Imp1*^{ΔIEC} ($n = 8$), *Atg7*^{ΔIEC} ($n = 5$), and *Imp1*^{ΔIEC}; *Atg7*^{ΔIEC} ($n = 7$) mice. At day 5, *Imp1*^{ΔIEC}; *Atg7*^{ΔIEC} mice lose significantly more weight as compared to control mice (P -value = 0.0076). Note that data for *Imp1*^{WT} and *Imp1*^{ΔIEC} mice from Fig 1 are presented here for comparison to *Atg7*^{ΔIEC} and *Imp1*^{ΔIEC}; *Atg7*^{ΔIEC} mice, which were performed in a separate cohort.

C Kaplan–Meier curve of the mice used in (B), demonstrating *Imp1*^{ΔIEC}; *Atg7*^{ΔIEC} mice become moribund prior to study endpoint during recovery from 3% DSS compared to controls (P -value = 0.0082).

D Representative images of blinded examination of small bowel and colon sections from aged *Imp1*^{WT} and *Imp1*^{ΔIEC}; *Atg7*^{ΔIEC} mice. *Imp1*^{ΔIEC}; *Atg7*^{ΔIEC} mice exhibited minimal foci of acute inflammation (neutrophils in < 5% of examined mucosa pointed by yellow arrows; Scale bar = 100 μ m).

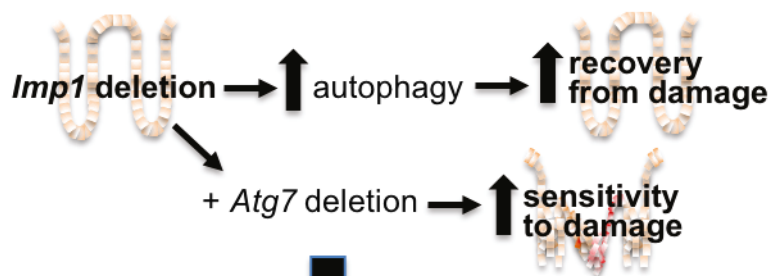
Data information: All data are expressed as mean \pm SEM. $**P < 0.01$. For DSS weights, significance was determined using the Mann–Whitney test. Cox regression was used to calculate statistical significance for Kaplan–Meier curves.

representing up to 3% of the transcriptome in HEK293 cells [36]. These granules contain significant enrichment of transcripts encoding proteins involved in ER quality control, Golgi, and secretory vesicles. Recent studies describe IMP1 localization in P-bodies, which house mRNAs involved in many regulatory processes that are transiently repressed [37]. This suggests that IMP1 may modulate repression of target mRNAs in certain contexts. In the present manuscript, we find that IMP1 deletion is associated with increased autophagy, which indicates a putative role for IMP1 to repress this pathway in intestinal epithelial cells (Fig 7). We

provide evidence for increased mRNA, protein, and translation efficiency of autophagy pathway components with IMP1 deletion suggesting that IMP1 could affect the autophagy pathway both transcriptionally and translationally, either directly or indirectly. Future studies are required to demonstrate whether IMP1 directly modulates translation of autophagy transcripts in the colonic epithelium.

We cannot exclude a role for IMP1 in regulating autophagy transcript stability. Recent eCLIP studies in human pluripotent stem cells (hPSCs) revealed IMP1 binding largely, but not

New findings:



Working model:

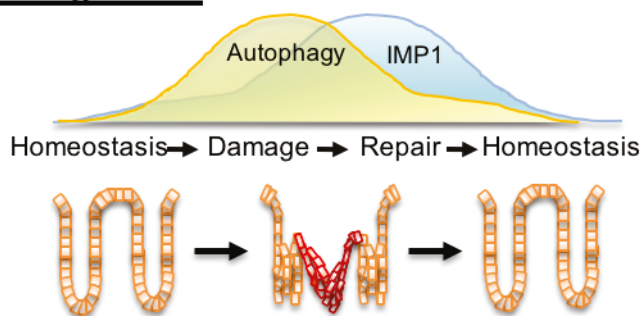


Figure 7. IMP1 contributes to colonic epithelial repair in part via modulation of autophagy.

We demonstrate that *Imp1* deletion enhances autophagy flux and promotes better recovery from DSS-induced damage. Deletion of *Atg7* in mice with *Imp1* deletion increases sensitivity to damage, suggesting that pathways regulated by *Imp1* may normally compensate for autophagy loss. These data contribute to a working model whereby dynamic regulation of *Imp1* during injury may serve to modulate autophagy during the reparative response.

exclusively, to 3'UTRs to regulate mRNA stability (Conway 26), whereas our analysis of this dataset revealed IMP1 binding to *ATG3* and *ATG5* transcripts at the 5'UTR. In addition, recent studies described a new role for IMP proteins as “readers” of N 6-methyladenosine (m⁶A) modified mRNAs [27]. This is intriguing, as emerging studies suggest that autophagy transcripts may be controlled by m⁶A modification [62]. It is therefore likely that IMP1 may modulate the autophagy pathway via multiple mechanisms, which provides one explanation as to why we observe direct binding of some, but not all autophagy transcripts in RIP assays for IMP1 in colon cancer cell lines.

In intestinal epithelial cells (IECs), autophagy can contribute to microbial regulation through packaging and secretion of lysozyme by Paneth cells [63]. Independent groups have demonstrated that mice with *Atg16l1* gene mutations are more sensitive to colitis or infection, exhibit increased serum IL-1β and IL-18, and display diffuse lysozyme staining in Paneth cells [42–47]. Evaluation of *Imp1^{ΔIEC}* mice revealed diffuse lysozyme staining. Recent studies have demonstrated that Paneth cells secrete lysozyme via secretory autophagy during bacterial infection through activation of dendritic cell-innate lymphoid cells circuit [63]; however, it remains unclear whether secretory autophagy is engaged as a homeostatic mechanism. As such, it would be interesting to determine whether IMP1 may regulate Paneth cell secretory autophagy in future studies, which could underlie its putative role in patients with inflammatory bowel disease. Our finding that *Atg7* deletion sensitizes *Imp1^{ΔIEC}*

mice to DSS together with data that *Imp1* is upregulated with *Atg7* deletion suggests a potential compensatory role for pathways regulated by IMP1 and autophagy. Prior studies have demonstrated that the ER stress pathway is upregulated in mice with autophagy deletion and that deletion of both pathways at the same time can promote spontaneous ileitis [60]. We therefore evaluated *Imp1^{ΔIEC}Atg7^{ΔIEC}* mice for evidence of spontaneous intestinal inflammation, but did not find any evidence of chronic enteritis in these mice.

We developed recently a transgenic mouse with intestinal epithelial *Imp1* overexpression [35] and found that these mice do not exhibit spontaneous inflammation (evaluated up to 16 months of age, unpublished). Therefore, our data demonstrating high IMP1 expression in patients with Crohn's disease and ulcerative colitis suggest that IMP1 may be upregulated as a consequence of chronic stress or inflammation rather than acting as an initiating factor. The upstream signaling pathways that regulate IMP1 expression in intestinal epithelial cells and the fate of IMP1-bound transcripts (stabilization versus degradation) during chronic inflammation are therefore a key area for future investigation. In summary, the current data contribute to a working model whereby IMP1 may function as a mediator of epithelial repair in part by modulating or compensating for autophagy aberrations in intestinal epithelial cells. More broadly, these studies underscore the importance of evaluating posttranscriptional contributions to gastrointestinal homeostasis and disease.

Materials and Methods

Human sample analyses

Frozen colon tissue and formalin-fixed paraffin-embedded (FFPE) samples from adult normal, Crohn's disease, and ulcerative colitis patients were obtained from the Cooperative Human Tissue Network (CHTN) via the University of Pennsylvania Center for Molecular Studies in Digestive and Liver Diseases Molecular Biology and Gene Expression Core. Patient demographics are listed in Table 1. RNA was extracted from frozen tissue using Trizol (Thermo Fisher, Waltham, MA). Publicly available RNA-sequencing data from the RISK cohort of pediatric ileal Crohn's [38] were evaluated for differential expression of IGF2BP1 (IMP1), IMP2, and IMP3. Sequenced reads were trimmed using Trim Galore! (version 0.4.4), and aligned to the GRCh37 reference genome using STAR, version 2.5.3a. Uniquely mapped reads were quantified by Ensembl gene IDs using featureCounts from Subread version 1.6.0. Lowly or unexpressed genes were removed from the analysis if they showed < 2 counts per million in < 5 samples across all conditions. Read counts were transformed with voom and evaluated for differential expression using limma. Immunohistochemistry for IMP1 in human tissue sections was performed using anti-IMP1 (Santa Cruz, sc-21026, Table EV4) using Animal-Free Blocker (Vector Laboratories).

Mice

Mice were cared for in accordance with University Laboratory Animal Resources requirements under an Institutional Animal Care and Use Committee-approved protocol. *VillinCre;Imp1-floxed* (*Imp1^{ΔIEC}*) mice were generated previously [32] and maintained on a C57Bl/6 background. Control mice had floxed, intact alleles (*Imp1^{WT}*). Male and female mice were both used at 8–12 weeks. *Atg7-floxed* mice were kindly provided by RIKEN BRC through National Bio-Resource Project of MEXT, Japan [59]. Genotyping primers are listed in Table EV2. Mice were housed in specific pathogen-free conditions and fed standard, irradiated chow and water *ad libitum*.

Co-housed control and experimental genotypes were randomized at weaning across multiple cages. Mice were given 3% or 5% dextran sodium sulfate (40,000–50,000 kDa molecular weight; Affymetrix CAS 9011-18-1) in drinking water for acute or 2.5% DSS for chronic colitis. During all experiments, body weights were recorded daily, and mice were euthanized before losing a maximum of 25% total body weight or if they began to show poor body condition. Mice that died or were euthanized prior to the study endpoint due to poor body condition were included in weight loss calculations where data points were available. Histological scoring was performed blinded by expert veterinary pathologist Enrico Radaelli and human pathologist Benjamin Wilkins according to published protocols [64]. Sample sizes were determined based upon the investigators' prior experience with specific models (KEH, GDW). Animal numbers are listed in Table EV3. Data for both sexes were combined and analyzed with specific statistical tests indicated in each figure legend.

For AOM/DSS tumor model, adult (8–12 weeks) male and female control and *Imp1^{ΔIEC}* mice were given a single intraperitoneal injection of azoxymethane (AOM, Sigma, St Louis, MO) at a dose of

10 mg/kg, followed by three cycles of 2.5% dextran sodium sulfate (DSS, Affymetrix, Santa Clara, CA) for 5 days in the drinking water *ad libitum* with 1 week of normal water in between each cycle. Mice were sacrificed 14 weeks after the AOM injection. A total of ≥ 14 mice per genotype were tested across two independent experiments. Upon sacrifice, gross colon lesions were evaluated in a blinded fashion (KEH) using a Nikon SMZ645 dissecting stereomicroscope.

qRT-PCR

Cell line, small intestine, or colon crypt epithelial RNA was isolated using GeneJet RNA purification kit (ThermoFisher). Equal amounts of total RNA were reverse-transcribed using Taqman RT Reagents kit and resulting cDNA used with Power SYBR Green PCR Master Mix (Applied Biosystems/ThermoFisher) or Taqman Fast Universal PCR Master Mix (Applied Biosystems/ThermoFisher) and validated primer sets (Table EV5). Non-reverse-transcribed samples were used as no RT controls. Gene expression was calculated using $R = 2^{(-\Delta\Delta C_t)}$ method, where changes in C_t values for the genes of interest were normalized to housekeeping genes. All experiments were replicated in at least three independent experiments with technical replicates (duplicates).

Histology

Small intestines were fixed in 10% formalin, processed, and paraffin-embedded. Immunofluorescence (IF) staining was performed using heat antigen-retrieval in citric acid buffer (pH 6.0) and staining with antibodies listed in Table EV4. For all staining, no-primary and/or biological negative controls (*Imp1^{ΔIEC}*) were used. Lysozyme scoring was performed according to published protocols [42,60] by a blinded investigator (ETL). Muc2 scoring was performed by counting the number of Muc2-positive in 10 high powered (10 \times) fields taken at random throughout the small intestinal epithelium. Images were taken and counted by an observer blinded to genotype (SFA). Counting was performed using the ImageJ Cell Counter plugin.

Transmission electron microscopy

Mouse small intestine tissues were fixed in cacodylate-buffered 2.5% (w/v) glutaraldehyde, post-fixed in 2.0% osmium tetroxide, and then embedded in epoxy resin and ultrathin sections post-stained in the University of Pennsylvania Electron Microscopy Resource Laboratory. Images were obtained using Jeol-1010 transmission electron microscope fitted with a Hamamatsu digital camera and AMT Advantage imaging software. A total of four mice per genotype were evaluated by two investigators for Paneth cell granule morphology and representative photographs presented (KEH and BJW) [53]. Image contrast was enhanced equally in all photographs.

Western blot

SW480 and Caco2 cells or isolated mouse epithelial cells were harvested in western lysis buffer (Cell Signaling #9803, 10 mM NaF, 1 mM Na₃VO₄, Halt protease cocktail ThermoFisher #78430), resolved in reducing conditions on 4–12% gradient gels, and

detected with ECL Prime Western Blotting Detection Reagent (Amersham; RPN2232). Antibodies are listed in Table EV4. Western blots were reproduced in at least three independent passages of cells representing individual experiments.

Autophagy analyses via CytoID

CytoID Autophagy Detection Kit (Enzo Life Sciences) was used to stain single cell suspensions of crypt-enriched intestinal epithelium (1:100 in DPBS supplemented with 10% FBS at 37°C for 30 min) and co-stained with DAPI (4',6-diamidino-2-phenylindole). Flow cytometry was performed using FACSCanto or LSR II cytometers (BD Biosciences) and FlowJo software (Tree Star). Unstained cells from each specimen were utilized to establish background fluorescence. The percent of CytoID-positive cells was determined in the live cell fraction (DAPI-negative). The geometric mean fluorescence intensity for live cells was determined for each specimen following subtraction of background fluorescence. Blinded analysis was utilized (KAW) [54,65].

Cell lines

Human colon cancer cell line SW480 (ATCC CCL-228) and Caco2 (ATCC HTB-37) cells were obtained from ATCC. Cells are tested for mycoplasma at least every 3 months. *IMP1* was deleted in SW480 cells by co-transfecting cells with *IMP1* CRISPR/Cas9 KO Plasmid (h) (Santa Cruz; sc-401703) and *IMP-1* HDR Plasmid (h) (Santa Cruz; sc-401703 HDR) followed by sorting and clonal expansion of RFP+ve cells.

Ribosome profiling

Ribosome profiling libraries from three pooled cell culture plates were prepared using a standard protocol [66], with minor modifications. Separate 5' and 3' linkers were ligated to the RNA-fragment instead of 3' linker followed by circularization [67]. 5' linkers contained four random nt unique molecular identifier (UMI) similar to a 5 nt UMI in 3' linkers. During size selection, we restricted the footprint lengths to 18–34 nts. Matched RNA-seq libraries were prepared using RNA that was randomly fragmentation by incubating for 15 min at 95°C with 1 mM EDTA, 6 mM Na₂CO₃, and 44 mM NaHCO₃, pH 9.3. RNA-seq fragments were restricted to 18–50 nts. Ribosomal rRNA was removed from pooled RNA-seq and footprinting samples using RiboZero (Epicenter MRZH116). cDNA for the pooled library was PCR-amplified for 15 cycles. RNA-seq and footprinting reads were mapped to the human transcriptome using the riboviz pipeline [68]. Complete TE analyses and pathway analyses are provided in Dataset EV1 and Table EV1, respectively.

Enteroid analyses

Crypt isolation and culture was performed as described previously [69]. An equal number of crypts were plated in 24-well plates at a density of 300 crypts per well in an 80/20 mixture of Matrigel Matrix (Corning) and complete media (containing 50 ng/ml mouse EGF (R&D Systems) and 2.5% Noggin/R-spondin conditioned media [70]. Enteroids were treated with 100 ng/ml Bafilomycin A

for 12 h and harvested using western lysis buffer. Two independent enteroid lines from each of *Imp1*^{WT} and *Imp1*^{ΔIEC} mice were generated and used at passage 1. *Imp1* knockout was confirmed by qPCR.

catRAPID analyses

We used the *catRAPID fragment* approach [71,72] to predict *IMP1* binding to autophagy-related transcripts (i.e., *MAP1LC3B*, *ATG3*, *BECN1*, *ATG5*, *ATG16L1*, and *ATG7*). *ACTB* and *TNFRSF1B/ITGA7* were also included as positive and negative controls, respectively. In our analysis, we included different isoforms for each transcript, for a total of 25 different targets, including the positive and negative controls (http://s.tartagliolab.com/page/catrapid_group).

Transcript score

Given a transcript isoform r_i , we used *catRAPID uniform fragmentation* to generate j overlapping fragments that cover the entire sequence. The fragments $r_{i,j}$ are then used to compute *catRAPID* interacting propensities with *IMP1* and IgG (negative control). We define the *interaction threshold* $\theta(r_i)$ as the highest interaction propensity score that IgG has with the j fragments generated from sequence r_i :

$$\theta(r_i) = \max_j [\pi(p = \text{IgG}, r = r_{i,j})] \quad (1)$$

For every *IMP1* interaction with fragments, we computed the *normalized interaction* π' by subtracting the interaction threshold of the corresponding transcript to the *catRAPID* interaction score.

$$\pi'(p = \text{IMP1}, r = r_{i,j}) = \pi(p = \text{IMP1}, r = r_{i,j}) - \theta(r_i) \quad (2)$$

Fragments with normalized interaction score $\pi' > 0$ are predicted to interact with *IMP1*. The *Isoform Score* of each isoform Π_i is computed as the average normalized interaction score of interacting fragments $\pi' > 0$ over the total number of fragments $n(i)$:

$$\Pi_i = \frac{1}{n(i)} \sum_j^{n(i)} \pi'(p = \text{IMP1}, r = r_{i,j}) \forall j: \pi'(p = \text{IMP1}, r = r_{i,j}) > 0 \quad (3)$$

We define the *Transcript Score* Π_r (Fig 5A) as a global interaction propensity of all isoforms belonging to a certain transcript. The *Transcript Score* is defined as the average of the *Isoform Scores* for all the isoforms analyzed for each transcript:

$$\Pi_r = \frac{1}{N(r)} \sum_i^{N(r)} \Pi_i \quad (4)$$

Where $N(r)$ is the number of isoforms considered for each transcript.

Ribonucleoprotein particle (RNP)-immunoprecipitation

RNP-immunoprecipitations (RIPs) were performed in Caco2 and SW480 cells using the RiboCluster Prolifer™ RIP-Assay Kit (Medical & Biological Laboratories) according to manufacturer's instructions.

Anti-IMP1 (MBL RN007P, which targets 561–577aa) or control IgG (supplied in kit) was used. Quality control samples for total protein and RNA input as well as immunoprecipitated proteins were evaluated for each experiment. Isolated RNA was reverse-transcribed using the Taqman RT Reagents kit and qPCR performed using the oligonucleotides listed in Table EV5. Raw C_t values from IMP1- and IgG- immunoprecipitated samples were used to determine “percent input” for each target, followed by dividing IMP1-immunoprecipitated signal by the respective IgG signal. Data for each individual target were then normalized to input and expressed as fold-enrichment relative to negative control targets *TNFRSF1B*. Positive control was previously identified IMP1 target *ACTB* [9,15]. Three independent RIP experiments were performed. Cells with IMP1 deletion were used as negative control.

Statistical analyses

Applying unpaired, two-tailed Student’s *t*-tests or one-way ANOVA, with $P < 0.05$ as statistically significant, determined statistical significance of comparisons between control and experimental conditions unless otherwise noted in the figure legends. For weight analyses in DSS experiments, statistical significance is determined using the non-parametric Mann–Whitney test. Cox regression was used to calculate statistical significance for Kaplan–Meier curves. For all analyses, unless noted otherwise, data from a minimum of three experiments are presented as mean \pm standard error of mean (SEM). Sample sizes for individual experiments, including biological and technical replicates, are described in each figure legend, as well as number of experimental replicates.

Expanded View for this article is available online.

Acknowledgements

We wish to thank Dr. Anil K. Rustgi (UPenn) and laboratory for support, discussions, and technical input. We thank UPenn Core Facilities: Molecular Pathology and Imaging, Human and Microbial Analytic Repository, Cell Culture/iPS, Flow Cytometry, and Electron Microscopy. We thank Dr. Donita Brady (UPenn) and laboratory for technical advice. We thank also Drs. T. Stappenbeck, A. Rodriguez, P. Vedula, L. Ghanem, and Y. Barash for discussions and advice. We thank Drs. Spiegelman and Noubissi for *Imp1*-floxed mice. Research reported in this publication was supported by the National Center for Advancing Translational Sciences of the National Institutes of Health under Award Number UL1TR001878. NIH K01DK100485 (KEH), Crohn’s and Colitis Foundation Career Development Award (KEH), NIH R03DK114463 (KEH); Institute for Translational Medicine and Therapeutics of the Perelman School of Medicine at the University of Pennsylvania (KEH); NIH P30DK050306 and its pilot grant program (KEH); start-up funds from the Children’s Hospital of Philadelphia Research Institute (KEH); NIH T32CA115299-09 (SFA); NIH R01DK056645 (PC, RM, SFA); NIH K08DK099379 (BJW); European Union Seventh Framework Programme (FP7/2007–2013), through the European Research Council and RIBOMY-LOME_309545 (GGT), the Spanish Ministry of Economy and Competitiveness (BFU2014-55054-P and fellowship to FCS), AGAUR (2014 SGR 00685), the Spanish Ministry of Economy and Competitiveness, Centro de Excelencia Severo Ochoa 2013–2017 (SEV-2012-0208), NIH F32DK107052 (SFA), NIH K01DK103953 (KAW), NIH R03DK118304 (KAW), HHMI Medical Research Fellows Program (ETL), and Fonds de Recherche en Santé du Québec (P-Giroux-27692 and P-Giroux-31601), NIH R01GM103591 (GDW), NIH R35GM124976 (SL, HRSW, PS), NIGMS T32GM008216-29 (SWF), start-up funds

from Human Genetics Institute of New Jersey and Rutgers University (SL, HRSW, PS).

Author contributions

Conceptualization: PC, KAW, KEH. Software and Formal Analyses: DSML, SL, HRSW, FCS, GGT, SM, PS. Investigation: PC, KAW, SFA, FCS, LAS, RM, ETL, SL, HRSW, SM, LC, PAW, LRP, VG, BJW, KEH. Writing-Original Draft: PC, KEH. Writing-Review and Editing: PC, PAW, KAW, SFA, GGT, PS, GDW, KEH. Funding acquisition: KEH.

Conflict of interest

The authors declare that they have no conflict of interest.

References

- Li N, Yousefi M, Nakauka-Ddamba A, Li F, Vandivier L, Parada K, Woo DH, Wang S, Naqvi AS, Rao S *et al* (2015) The Msi family of RNA-binding proteins function redundantly as intestinal oncoproteins. *Cell Rep* 13: 2440–2455
- Wang S, Li N, Yousefi M, Nakauka-Ddamba A, Li F, Parada K, Rao S, Minuesa G, Katz Y, Gregory BD *et al* (2015) Transformation of the intestinal epithelium by the MSI2 RNA-binding protein. *Nat Commun* 6: 6517
- Madison BB, Liu Q, Zhong X, Hahn CM, Lin N, Emmett MJ, Stanger BZ, Lee JS, Rustgi AK (2013) LIN28B promotes growth and tumorigenesis of the intestinal epithelium via Let-7. *Genes Dev* 27: 2233–2245
- Madison BB, Jeganathan AN, Mizuno R, Winslow MM, Castells A, Cuatrecasas M, Rustgi AK (2015) Let-7 represses carcinogenesis and a stem cell phenotype in the intestine via regulation of Hmga2. *PLoS Genet* 11: e1005408
- Tu HC, Schwitalla S, Qian Z, LaPier GS, Yermalovich A, Ku YC, Chen SC, Viswanathan SR, Zhu H, Nishihara R *et al* (2015) LIN28 cooperates with WNT signaling to drive invasive intestinal and colorectal adenocarcinoma in mice and humans. *Genes Dev* 29: 1074–1086
- Yousefi M, Li N, Nakauka-Ddamba A, Wang S, Davidow K, Schoenberger J, Yu Z, Jensen ST, Kharas MG, Lengner CJ (2016) Msi RNA-binding proteins control reserve intestinal stem cell quiescence. *J Cell Biol* 215: 401–413
- Parham LR, Williams PA, Chatterji P, Whelan KA, Hamilton KE (2018) RNA regulons are essential in intestinal homeostasis. *Am J Physiol Gastrointest Liver Physiol* 316: G197–G204
- Nielsen J, Christiansen J, Lykke-Andersen J, Johnsen AH, Wewer UM, Nielsen FC (1999) A family of insulin-like growth factor II mRNA-binding proteins represses translation in late development. *Mol Cell Biol* 19: 1262–1270
- Ross AF, Oleynikov Y, Kislauskis EH, Taneja KL, Singer RH (1997) Characterization of a beta-actin mRNA zipcode-binding protein. *Mol Cell Biol* 17: 2158–2165
- Leeds P, Kren BT, Boylan JM, Betz NA, Steer CJ, Gruppiso PA, Ross J (1997) Developmental regulation of CRD-BP, an RNA-binding protein that stabilizes *c-myc* mRNA *in vitro*. *Oncogene* 14: 1279–1286
- Runge S, Nielsen FC, Nielsen J, Lykke-Andersen J, Wewer UM, Christiansen J (2000) H19 RNA binds four molecules of insulin-like growth factor II mRNA-binding protein. *J Biol Chem* 275: 29562–29569
- Lemm I, Ross J (2002) Regulation of *c-myc* mRNA decay by translational pausing in a coding region instability determinant. *Mol Cell Biol* 22: 3959–3969

13. Vikesaa J, Hansen TV, Jonson L, Borup R, Wewer UM, Christiansen J, Nielsen FC (2006) RNA-binding IMPs promote cell adhesion and invadopodia formation. *EMBO J* 25: 1456–1468
14. Noubissi FK, Goswami S, Sanek NA, Kawakami K, Minamoto T, Moser A, Grinblat Y, Spiegelman VS (2009) Wnt signaling stimulates transcriptional outcome of the Hedgehog pathway by stabilizing GLI1 mRNA. *Cancer Res* 69: 8572–8578
15. Manieri NA, Drylewicz MR, Miyoshi H, Stappenbeck TS (2012) Igf2 bp1 is required for full induction of Ptg2 mRNA in colonic mesenchymal stem cells in mice. *Gastroenterology* 143: 110–121.e10
16. Huttelmaier S, Zenklusen D, Lederer M, Dichtenberg J, Lorenz M, Meng X, Bassell CJ, Condeelis J, Singer RH (2005) Spatial regulation of beta-actin translation by Src-dependent phosphorylation of ZBP1. *Nature* 438: 512–515
17. Stohr N, Kohn M, Lederer M, Glass M, Reinke C, Singer RH, Huttelmaier S (2012) IGF2BP1 promotes cell migration by regulating MK5 and PTEN signaling. *Genes Dev* 26: 176–189
18. Stohr N, Lederer M, Reinke C, Meyer S, Hatzfeld M, Singer RH, Huttelmaier S (2006) ZBP1 regulates mRNA stability during cellular stress. *J Cell Biol* 175: 527–534
19. Noubissi FK, Elcheva I, Bhatia N, Shakoori A, Ougolkov A, Liu J, Minamoto T, Ross J, Fuchs SY, Spiegelman VS (2006) CRD-BP mediates stabilization of betaTrCP1 and c-myc mRNA in response to beta-catenin signalling. *Nature* 441: 898–901
20. Elcheva I, Goswami S, Noubissi FK, Spiegelman VS (2009) CRD-BP protects the coding region of betaTrCP1 mRNA from miR-183-mediated degradation. *Mol Cell* 35: 240–246
21. Bernstein PL, Herrick DJ, Prokipcak RD, Ross J (1992) Control of c-myc mRNA half-life *in vitro* by a protein capable of binding to a coding region stability determinant. *Genes Dev* 6: 642–654
22. Weidensdorfer D, Stohr N, Baude A, Lederer M, Kohn M, Schierhorn A, Buchmeier S, Wahle E, Huttelmaier S (2009) Control of c-myc mRNA stability by IGF2BP1-associated cytoplasmic RNPs. *RNA* 15: 104–115
23. Gu W, Wells AL, Pan F, Singer RH (2008) Feedback regulation between zipcode binding protein 1 and beta-catenin mRNAs in breast cancer cells. *Mol Cell Biol* 28: 4963–4974
24. Gu W, Katz Z, Wu B, Park HY, Li D, Lin S, Wells AL, Singer RH (2012) Regulation of local expression of cell adhesion and motility-related mRNAs in breast cancer cells by IMP1/ZBP1. *J Cell Sci* 125: 81–91
25. Hafner M, Landthaler M, Burger L, Khorshid M, Haussler J, Berninger P, Rothballer A, Ascano M Jr, Jungkamp AC, Munschauer M et al (2010) Transcriptome-wide identification of RNA-binding protein and microRNA target sites by PAR-CLIP. *Cell* 141: 129–141
26. Conway AE, Van Nostrand EL, Pratt GA, Aigner S, Wilbert ML, Sundararaman B, Freese P, Lambert NJ, Sathe S, Liang TY et al (2016) Enhanced CLIP uncovers IMP Protein-RNA targets in human pluripotent stem cells important for cell adhesion and survival. *Cell Rep* 15: 666–679
27. Huang H, Weng H, Sun W, Qin X, Shi H, Wu H, Zhao BS, Mesquita A, Liu C, Yuan CL et al (2018) Recognition of RNA N(6)-methyladenosine by IGF2BP proteins enhances mRNA stability and translation. *Nat Cell Biol* 20: 285–295
28. Hansen TV, Hammer NA, Nielsen J, Madsen M, Dalbaeck C, Wewer UM, Christiansen J, Nielsen FC (2004) Dwarfism and impaired gut development in insulin-like growth factor II mRNA-binding protein 1-deficient mice. *Mol Cell Biol* 24: 4448–4464
29. Fakhraldeen SA, Clark RJ, Roopra A, Chin EN, Huang W, Castorino J, Wisinski KB, Kim T, Spiegelman VS, Alexander CM (2015) Two isoforms of the RNA binding protein, coding region determinant-binding protein (CRD-BP/IGF2BP1), are expressed in breast epithelium, and support clonogenic growth of breast tumor cells. *J Biol Chem* 290: 13386–13400
30. Nishino J, Kim S, Zhu Y, Zhu H, Morrison SJ (2013) A network of heterochronic genes including Imp1 regulates temporal changes in stem cell properties. *Elife* 2: e00924
31. Dimitriadis E, Trangas T, Milatos S, Foukas PG, Gioulbasanis I, Curtis N, Nielsen FC, Pandis N, Dafni U, Bardi G et al (2007) Expression of oncofetal RNA-binding protein CRD-BP/IMP1 predicts clinical outcome in colon cancer. *Int J Cancer* 121: 486–494
32. Hamilton KE, Noubissi FK, Katti PS, Hahn CM, Davey SR, Lundsmith ET, Klein-Szanto AJ, Rhim AD, Spiegelman VS, Rustgi AK (2013) IMP1 promotes tumor growth, dissemination and a tumor-initiating cell phenotype in colorectal cancer cell xenografts. *Carcinogenesis* 34: 2647–2654
33. Hamilton KE, Chatterji P, Lundsmith ET, Andres SF, Giroux V, Hicks PD, Noubissi FK, Spiegelman VS, Rustgi AK (2015) Loss of stromal IMP1 promotes a tumorigenic microenvironment in the colon. *Mol Cancer Res* 13: 1478–1486
34. Degrauwe N, Suva ML, Janiszewska M, Riggi N, Stamenkovic I (2016) IMPs: an RNA-binding protein family that provides a link between stem cell maintenance in normal development and cancer. *Genes Dev* 30: 2459–2474
35. Chatterji P, Hamilton KE, Liang S, Andres SF, Wijeratne HRS, Mizuno R, Simon LA, Hicks PD, Foley SW, Pitarresi JR et al (2018) The LIN28B-IMP1 post-transcriptional regulon has opposing effects on oncogenic signaling in the intestine. *Genes Dev* 32: 1020–1034
36. Jonson L, Vikesaa J, Krogh A, Nielsen LK, Hansen T, Borup R, Johnsen AH, Christiansen J, Nielsen FC (2007) Molecular composition of IMP1 ribonucleoprotein granules. *Mol Cell Proteomics* 6: 798–811
37. Hubstenberger A, Courel M, Benard M, Souquere S, Ernoult-Lange M, Chouaib R, Yi Z, Morlot JB, Munier A, Fradet M et al (2017) P-body purification reveals the condensation of repressed mRNA regulons. *Mol Cell* 68: 144–157.e5
38. Haberman Y, Tickle TL, Dexheimer PJ, Kim MO, Tang D, Karns R, Baldasano RN, Noe JD, Rosh J, Markowitz J et al (2014) Pediatric Crohn disease patients exhibit specific ileal transcriptome and microbiome signature. *J Clin Invest* 124: 3617–3633
39. Huber S, Gagliani N, Zenewicz LA, Huber FJ, Bosurgi L, Hu B, Hedl M, Zhang W, O'Connor W Jr, Murphy AJ et al (2012) IL-22BP is regulated by the inflammasome and modulates tumorigenesis in the intestine. *Nature* 491: 259–263
40. Zhong Y, Karaletsos T, Drewe P, Sreedharan VT, Kuo D, Singh K, Wendel HG, Ratsch G (2017) RiboDiff: detecting changes of mRNA translation efficiency from ribosome footprints. *Bioinformatics* 33: 139–141
41. Chen J, Bardes EE, Aronow BJ, Jegga AG (2009) ToppGene Suite for gene list enrichment analysis and candidate gene prioritization. *Nucleic Acids Res* 37: W305–W311
42. Cadwell K, Liu JY, Brown SL, Miyoshi H, Loh J, Lennerz JK, Kishi C, Kc W, Carrero JA, Hunt S et al (2008) A key role for autophagy and the autophagy gene Atg16 L1 in mouse and human intestinal Paneth cells. *Nature* 456: 259–263
43. Cadwell K, Patel KK, Komatsu M, Virgin IV HW, Stappenbeck TS (2009) A common role for Atg16L1, Atg5 and Atg7 in small intestinal Paneth cells and Crohn disease. *Autophagy* 5: 250–252
44. Saitoh T, Fujita N, Jang MH, Uematsu S, Yang BG, Satoh T, Omori H, Noda T, Yamamoto N, Komatsu M et al (2008) Loss of the autophagy protein Atg16L1 enhances endotoxin-induced IL-1beta production. *Nature* 456: 264–268

45. Pott J, Kabat AM, Maloy KJ (2018) Intestinal epithelial cell autophagy is required to protect against TNF-induced apoptosis during chronic colitis in mice. *Cell Host Microbe* 23: 191–202.e4
46. Burger E, Araujo A, Lopez-Yglesias A, Rajala MW, Geng L, Levine B, Hooper LV, Burstein E, Yarovinsky F (2018) Loss of Paneth cell autophagy causes acute susceptibility to *Toxoplasma gondii*-mediated inflammation. *Cell Host Microbe* 23: 177–190.e4
47. Matsuzawa-Ishimoto Y, Shono Y, Gomez LE, Hubbard-Lucey VM, Cammer M, Neil J, Dewan MZ, Lieberman SR, Lazrak A, Marinis JM et al (2017) Autophagy protein ATG16L1 prevents necroptosis in the intestinal epithelium. *J Exp Med* 214: 3687–3705
48. VanDussen KL, Liu TC, Li D, Towfic F, Modiano N, Winter R, Haritunians T, Taylor KD, Dhall D, Targan SR et al (2014) Genetic variants synthesize to produce paneth cell phenotypes that define subtypes of Crohn's disease. *Gastroenterology* 146: 200–209
49. Liu TC, Gurram B, Baldridge MT, Head R, Lam V, Luo C, Cao Y, Simpson P, Hayward M, Holtz ML et al (2016) Paneth cell defects in Crohn's disease patients promote dysbiosis. *JCI Insight* 1: e86907
50. Liu TC, Gao F, McGovern DP, Stappenbeck TS (2014) Spatial and temporal stability of paneth cell phenotypes in Crohn's disease: implications for prognostic cellular biomarker development. *Inflamm Bowel Dis* 20: 646–651
51. Liu TC, Naito T, Liu Z, VanDussen KL, Haritunians T, Li D, Endo K, Kawai Y, Nagasaki M, Kinouchi Y et al (2017) LRRK2 but not ATG16L1 is associated with Paneth cell defect in Japanese Crohn's disease patients. *JCI Insight* 2: e91917
52. Stappenbeck TS, McGovern DPB (2017) Paneth cell alterations in the development and phenotype of Crohn's disease. *Gastroenterology* 152: 322–326
53. Klionsky DJ, Abdelmohsen K, Abe A, Abedin MJ, Abeliovich H, Acevedo Arozena A, Adachi H, Adams CM, Adams PD, Adeli K et al (2016) Guidelines for the use and interpretation of assays for monitoring autophagy (3rd edition). *Autophagy* 12: 1–222
54. Whelan KA, Merves JF, Giroux V, Tanaka K, Guo A, Chandramouleeswaran PM, Benitez AJ, Dods K, Que J, Masterson JC et al (2017) Autophagy mediates epithelial cytoprotection in eosinophilic oesophagitis. *Gut* 66: 1197–1207
55. Whelan KA, Merves JF, Giroux V, Tanaka K, Guo A, Chandramouleeswaran PM, Benitez AJ, Dods K, Que J, Masterson JC et al (2016) Autophagy mediates epithelial cytoprotection in eosinophilic oesophagitis. *Gut* 66: 1197–1207
56. Kijima T, Nakagawa H, Shimonosono M, Chandramouleeswaran PM, Hara T, Sahu V, Kasagi Y, Kikuchi O, Tanaka K, Giroux V et al (2019) Three-dimensional organoids reveal therapy resistance of esophageal and oropharyngeal squamous cell carcinoma cells. *Cell Mol Gastroenterol Hepatol* 7: 73–91
57. Ascano M, Hafner M, Cekan P, Gerstberger S, Tuschl T (2012) Identification of RNA-protein interaction networks using PAR-CLIP. *Wiley Interdiscip Rev RNA* 3: 159–177
58. Cirillo D, Blanco M, Armaos A, Bunes A, Avner P, Guttman M, Cerase A, Tartaglia GG (2016) Quantitative predictions of protein interactions with long noncoding RNAs. *Nat Methods* 14: 5–6
59. Komatsu M, Waguri S, Ueno T, Iwata J, Murata S, Tanida I, Ezaki J, Mizushima N, Ohsumi Y, Uchiyama Y et al (2005) Impairment of starvation-induced and constitutive autophagy in Atg7-deficient mice. *J Cell Biol* 169: 425–434
60. Adolph TE, Tomczak MF, Niederreiter L, Ko HJ, Bock J, Martinez-Naves E, Glickman JN, Tschurtschenthaler M, Hartwig J, Hosomi S et al (2013) Paneth cells as a site of origin for intestinal inflammation. *Nature* 503: 272–276
61. Tsuboi K, Nishitani M, Takakura A, Imai Y, Komatsu M, Kawashima H (2015) Autophagy protects against colitis by the maintenance of normal gut microflora and secretion of mucus. *J Biol Chem* 290: 20511–20526
62. Jin S, Zhang X, Miao Y, Liang P, Zhu K, She Y, Wu Y, Liu DA, Huang J, Ren J et al (2018) m6A RNA modification controls autophagy through upregulating ULK1 protein abundance. *Cell Res* 28: 955–957
63. Bel S, Pendse M, Wang Y, Li Y, Ruhn KA, Hassell B, Leal T, Winter SE, Xavier RJ, Hooper LV (2017) Paneth cells secrete lysozyme via secretory autophagy during bacterial infection of the intestine. *Science* 357: 1047–1052
64. Washington MK, Powell AE, Sullivan R, Sundberg JP, Wright N, Coffey RJ, Dove WF (2013) Pathology of rodent models of intestinal cancer: progress report and recommendations. *Gastroenterology* 144: 705–717
65. Merves JF, Whelan KA, Benitez AJ, Muir AB, Furuta GT, Wang ML, Falk GW, Spergel JM, Nakagawa H (2016) ATG7 gene expression as a novel tissue biomarker in eosinophilic esophagitis. *Am J Gastroenterol* 111: 151–153
66. McGlincy NJ, Ingolia NT (2017) Transcriptome-wide measurement of translation by ribosome profiling. *Methods* 126: 112–129
67. Subtelny AO, Eichhorn SW, Chen GR, Sive H, Bartel DP (2014) Poly(A)-tail profiling reveals an embryonic switch in translational control. *Nature* 508: 66–71
68. Carja O, Xing T, Wallace EWJ, Plotkin JB, Shah P (2017) riboviz: analysis and visualization of ribosome profiling datasets. *BMC Bioinformatics* 18: 461
69. Hamilton KE, Crissey MA, Lynch JP, Rustgi AK (2015) Culturing adult stem cells from mouse small intestinal crypts. *Cold Spring Harb Protoc* 2015: 354–358
70. Sato T, Vries RG, Snippert HJ, van de Wetering M, Barker N, Stange DE, van Es JH, Abo A, Kujala P, Peters PJ et al (2009) Single Lgr5 stem cells build crypt-villus structures *in vitro* without a mesenchymal niche. *Nature* 459: 262–265
71. Bellucci M, Agostini F, Masin M, Tartaglia GG (2011) Predicting protein associations with long noncoding RNAs. *Nat Methods* 8: 444–445
72. Cirillo D, Agostini F, Klus P, Marchese D, Rodriguez S, Bolognesi B, Tartaglia GG (2013) Neurodegenerative diseases: quantitative predictions of protein-RNA interactions. *RNA* 19: 129–140